Braz J Phys (2014) 44:753–764
DOI 10.1007/s13538-014-0273-z

GENERAL AND APPLIED PHYSICS

Structural Modifications and Clustering of Low-Density Lipoproteins in Solution Induced by Heating

Cristiano L. P. Oliveira · Andrea M. Monteiro · Antonio M. Figueiredo Neto

Received: 30 July 2014 / Published online: 21 October 2014

Abstract This work presents a systematic study of low-density lipoprotein (LDL) in solutions subjected to subtle temperature changes, monitored by small angle X-ray scattering. From the data analysis, information about the equilibrium aggregation of the particles, as well as changes on the internal structure of the lipoproteins, were observed. The electron density profiles of the LDL particles were retrieved with a recently developed deconvolution method. Our results indicate that LDL particles keep their structure in the temperature range from about 22 °C up to 60 °C. Moreover, the formation of aggregates and their evolution as a function of time were monitored. Interestingly, when the temperature is raised to 80 °C, the results indicate the rupture of the particle and unspecific aggregation.

Keywords Lipoproteins · Temperature · Aggregation · SAXS · Modeling · LDL

1 Introduction

Plasma lipoproteins are heterogeneous particles of different sizes, composition, and density, whose main function is the cholesterol transport. These particles are constituted of a non-polar core, composed of triglycerides and cholesterol esters, surrounded by a monolayer of phospholipids, free cholesterol, and apolipoproteins (apo). High levels of the low-density lipoprotein (LDL), known as "bad cholesterol," are associated with high risk in developing a cardiovascular disease. The LDL is a particle rich in cholesterol ester and poor in triglycerides and free cholesterol. Moreover, each LDL particle contains only one macromolecule of apolipoprotein B100 (apoB-100), which is responsible for the integrity of the particle and metabolism. The LDL structure is very sensitive to changes in the environment, and this may alter its function. The mechanism by which LDL in vivo is modified is not yet completely understood. In a recent publication [1], the changes on the internal structure of LDL and HDL, due to in vitro oxidation by Cupper, were described. Also, the apo-B100 structure has been shown to be highly sensitive to chemical modification, such as oxidation induced by free radicals, and to temperature changes [2]. Thereby, the conformation of apo-B100 could be modified at higher temperatures, which would affect its recognition by the LDL cell receptors [3].

Scattering methods allow the study of the particles directly in solution. Investigations on the LDL structure as a function of the temperature by using scattering methods were performed in the 1970s by the seminal works of Deckelbaum, Laggner, and Atkinson [4–6], and more recently by Laggner and co-workers [2]. However, in all these cases, the data analysis is limited due to the presence of aggregates (induced by the temperature increase) and also by the problems on the retrieval of trustful scattering-length density profile for the lipoproteins from the scattering data. In a recent work, Jayaraman and co-workers investigated the thermal stability of LDL by using different techniques including calorimetric, circular dichroism, fluorescence, turbidity, and electron microscopic [7]. Their data show that thermal disruption of LDL involves irreversible changes in the particle with the release of neutral lipid from LDL core which coalesce into droplets. Gursky and co-workers [8] made quantitative kinetic analysis of thermal stability of LDL suggesting that fusion of LDL is preceded by other structural changes.

In this work, we present a systematic study of the changes in the structure of native LDL induced by subtle changes in

C. L. P. Oliveira · A. M. Monteiro · A. M. F. Neto
Instituto de Física, Universidade de São Paulo, São Paulo, Brazil

C. L. P. Oliveira (✉)
Institute of Physics, University of São Paulo, P.O. box 66318, 05314-970 São Paulo, SP, Brazil
e-mail: crislpo@if.usp.br

the temperature. Synchrotron radiation small-angle X-ray scattering data was collected for a series of LDL samples, and by using advanced modeling methods [1], information about the formation of aggregates, changes on the internal structure of the LDL particle, and modifications on the APO B conformation were obtained.

2 Materials and Methods

2.1 Isolation of LDL

The purification of LDL particles was described elsewhere [1]. Shortly, blood was drawn from of healthy normolipidemic donors, and the plasma was obtained after centrifugation at 1,000×*g* at 4 ° C, for 15 min. Benzamidine (2 mM), chloramphenicol (0.25 %), pheny-methyl-sulfonyfluoride (0.5 mM), gentamicin (0.5 %), and aprotinin (0.1 U/ml) were added to the plasma. LDL (1.006 < d < 1.063 mg/dl) was isolated in a sequential ultracentrifugation [9] process at 10^5x*g* at 4 °C, using the rotor of an ultracentrifuge (Hitachi Ultracentrifuge—Japan). The obtained samples were dialyzed for 24 h at 4 °C against phosphate buffered saline (PBS), pH 7.4. Later, the samples were put through a filter with micrometer pore (Milipore—Germany) and the protein concentration was determined using bicinchoninic acid protein assay kit (Pierce, USA), with bovine serum albumin as standard. The final LDL concentration was 1.3 mg/ml.

2.2 SAXS

LDL SAXS measurements were performed at the Brazilian Synchrotron Light Laboratory at the SAXS1 beamline [10]. The sample holder [11], a cell with dimensions 1×4×8 mm^3, was placed in a device coupled to a water-circulating thermal bath, enabling LDL solution samples measurements at controlled temperature. The wavelength of the incoming monochromatic X-ray beam was λ=1.48 Å and the distance between the sample and the detector was set to 3,200 mm, providing a q (scattering-vector modulus) interval from 0.006 to 0.25 $Å^{-1}$, where $q=4\pi(\sin\theta)/\lambda$ and 2θ is the scattering angle. The 2D scattering data was collected on a Dectris Pilatus™ 300k detector, and the integration of the SAXS patterns and data treatment were done with the FIT2D software [12]. Error estimation and normalization to absolute scale were performed by using the SUPERSAXS package [Oliveira and Pedersen, unpublished]. A rectangular beam with dimensions 300×100 microns was used. This beam size is further convoluted with the detector resolution of 172 microns. The experimental setup provided a resolution in q values of $\Delta q=0.00042$ $Å^{-1}$.

Data were collected at the temperatures: 22 °C (room temperature), 42 °C, 60 °C, and 80 °C. For the measurement at room temperature only 5 frames were obtained since the sample was stable over time. For the experiments at higher temperatures, the data collection was performed as follows: after the system reaches the thermal equilibrium (which is measured directly on the sample holder and monitored remotely), a fresh LDL sample is injected inside the sample holder and the measurement is started immediately after injection. Several (up to 5) 1 min frames were collected at 0, 5, 10, 20, 40, 60, and 80 min after injection. In all the cases, the frames were compared and averaged in order to have a single dataset representing each temperature. After the measurement on a given temperature, the cell is clean and the PBS buffer is measured at the same conditions and temperature for a proper background subtraction. For each temperature, a new fresh LDL sample was used.

The series of treated data is shown in Fig. 1.

2.3 Initial SAXS Data Analysis and Decoupling of the Form and Structure Factors

The analysis of the SAXS data was performed in several steps. At first, the data was analyzed by the Indirect Fourier Transformation method—IFT [13], with a slightly different implementation [14, 15]. From these analyses, coarse information about the size, shape, and aggregation behavior are obtained. Even the fresh LDL solution sample at room temperature shows the presence of a small fraction of particle's aggregates. The number of aggregates was shown to increase for increasing temperatures. In order to correctly analyze the contribution from the isolated LDL particles and the aggregates separately, it is necessary to decouple the form factor and structure factor of the scattering data. This was possible by using the Generalized indirect Fourier Transformation Method—GIFT [14]. We used a theoretical function for the structure factor contribution, and by the simultaneous optimization of the $p(r)$ function (form factor) and structure factor parameters, it was possible to obtain the theoretical form factor (without the structure factor contribution) and also a reliable structure factor function. In this approach, the scattering intensity $I(q)$ and structure factor $S(q)$ are given by:

$$I(q) = P(q)S(q) \tag{1}$$

$$S(q) = 1 + S_C^{agg}\exp\left[-\frac{q^2 R_G^{agg\,2}}{3}\right] \tag{2}$$

The form factor $P(q)$ is described by a set of spline functions, which are related to the pair distance distribution function $p(r)$ of the single particle by a Fourier transform [13]. For the structure factor $S(q)$, several different models were tested, but the data series were reasonably described by a simple model, which assumes that, at low angles, there is a Guinier Law for a particle (or aggregate) with radius of gyration $R_G{}^{agg}$, as shown in Eq. 2. In this model, the scale factor S_C^{agg} gives an

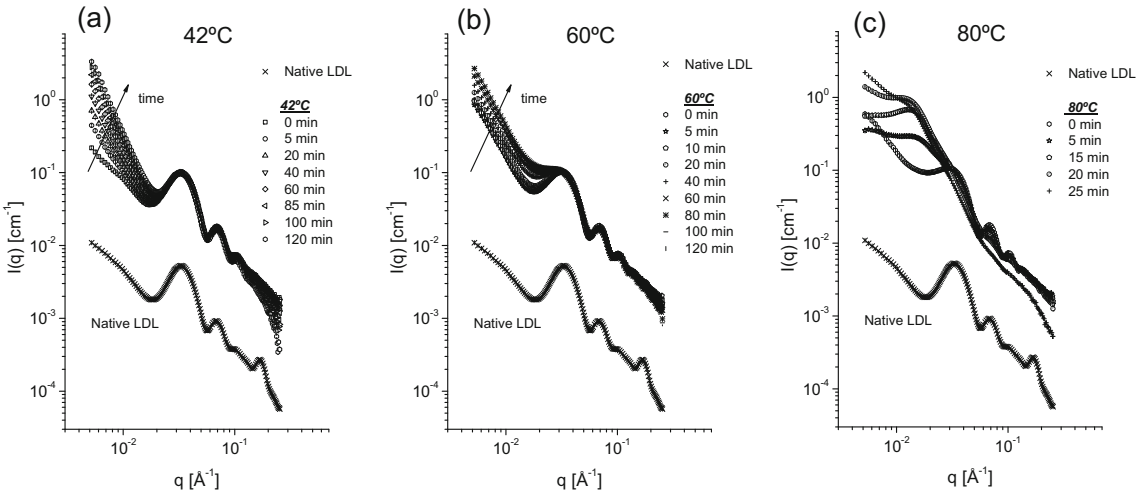

Fig. 1 SAXS data for the full series of measurements. **a** Data at 42 °C. **b** Data at 60 °C. **c** Data at 80 °C. In all the cases, the scattering data of the native LDL measured at 22 °C is shown for comparison. This *curve* is shifted for a better visualization

indication of the fraction of isolated particles and aggregates in the system, as described in the next section. As a result from these analyses, a good approximation for the form factor of the isolated particles and the structure factor of the aggregates were obtained.

2.4 Modeling of Aggregates and Evolution of the Aggregation Fraction

The description of the structure factor as an averaged radius of gyration for the aggregates allows the calculation of the "theoretical" scattering intensity of the aggregates by the simple extrapolation of the Guinier law to very small q values. From this curve, it is possible to obtain a pair-distance distribution curve, which may provide some general indications on the size and shape of the aggregates. Even though this procedure intrinsically assumes that the aggregates are globular, it provides some indications about the overall size and shape of the aggregates. Additionally, one can use an ab initio procedure to retrieve possible 3D shapes for the aggregates. This can be performed by the dummy atom modeling approach (Program DAMMIN [16]). Since one can assume that the aggregates are composed by isolated LDL particles, in this modeling, we used the radius of the dummy atoms similar to the average radius of the lipoproteins. In this framework, the obtained model for the aggregates is a direct indication of how the lipoproteins are arranged.

From the modeling results, it is also possible to follow the evolution of the fraction of aggregates in the sample. For this calculation, one can assume a simple two-component system: isolated LDL particles and aggregates. If there is only these two species in the sample, we have:

$$I(q)_{tot} = I(q)_{LDL} + I(q)_{Agg} \tag{3}$$

For a system of particles, the forward scattering is given by:

$$I(0) = c(\Delta\rho)^2 V^2 \tag{4}$$

where c is the concentration of particles, $\Delta\rho$ is the scattering length-density contrast, and V is the particle volume. Substituting Eq. 4 in Eq. 3, we have:

$$I(0)_{tot} = c_{LDL}(\Delta\rho)^2 V_{LDL}^2 + c_{agg}(\Delta\rho)^2 V_{agg}^2 \tag{5}$$

$$I(0)_{tot} = c_{LDL}(\Delta\rho)^2 V_{LDL}^2 \left(1 + \frac{c_{agg} V_{agg}^2}{c_{LDL} V_{LDL}^2}\right) \tag{6}$$

If one compares Eq. 6 with Eq. 2, one finds that:

$$S_C^{agg} = \frac{c_{agg} V_{agg}^2}{c_{LDL} V_{LDL}^2} \tag{7}$$

As demonstrated in the Appendix 1, it is possible to describe the numerical, volume, and intensity fraction of aggregates and isolated particles as a function of the scale factor S_C^{agg} and the radii of gyration of the isolated particles R_G^{LDL} and aggregates R_G^{agg}:

$$f_{LDL}^i = \frac{1}{1 + S_C^{agg}\left(\frac{R_G^{LDL}}{R_G^{agg}}\right)^{3\alpha}} \tag{8}$$

$$f_{agg}^i = \frac{1}{1 + \frac{1}{S_C^{agg}}\left(\frac{R_G^{agg}}{R_G^{LDL}}\right)^{3\alpha}} \tag{9}$$

So, we have for the numerical fraction i="num" and α=2, for the volume fraction i="vol" and α=1 and for the intensity fraction i="int" and α=0. The meaning of these fractions is related to the weighting of the calculation for each fraction.

The numerical fraction has no weighting, the volume fraction is weighted by the particle volumes, and the intensity fraction is weighted by the volume squared. The latter receives this name because the scattering intensity (Eq. 4) is weighted by the volume square, and therefore, this fraction provides the contribution to the final intensity.

Therefore, from the modeling (Eqs. 1 and 2) and estimations for the radius of gyration of the LDL particles and aggregates (which are also obtained from the fitting), one can retrieve the numerical, volume, and intensity fractions for the monomers and the aggregates for each dataset.

2.5 Modeling of LDL Single Particle

The complete description of the modeling procedure is found elsewhere [1]. In short, after having the form factors for each case, one can apply a deconvolution method, which fits the scattering data directly, allowing the inclusion of additional parameters as anisotropy and polydispersity, as well as to perform a simultaneous fitting of the background and other contributions. The particle is modeled as an ellipsoid of revolution with superimposed concentric shells of different electron densities. The parameters of these shells define the final radial profile. The polydispersity is included by integration of the form factor on a given size distribution. An additional term in the intensity is included in order to account for the contribution from flexible parts in the scatterers. The final expression that is used to fit the scattering data is given by:

$$I(q) = S_{C_1} P_{MOD}(q) + S_{C_2} P_{Deb}(q) + Back \tag{10}$$

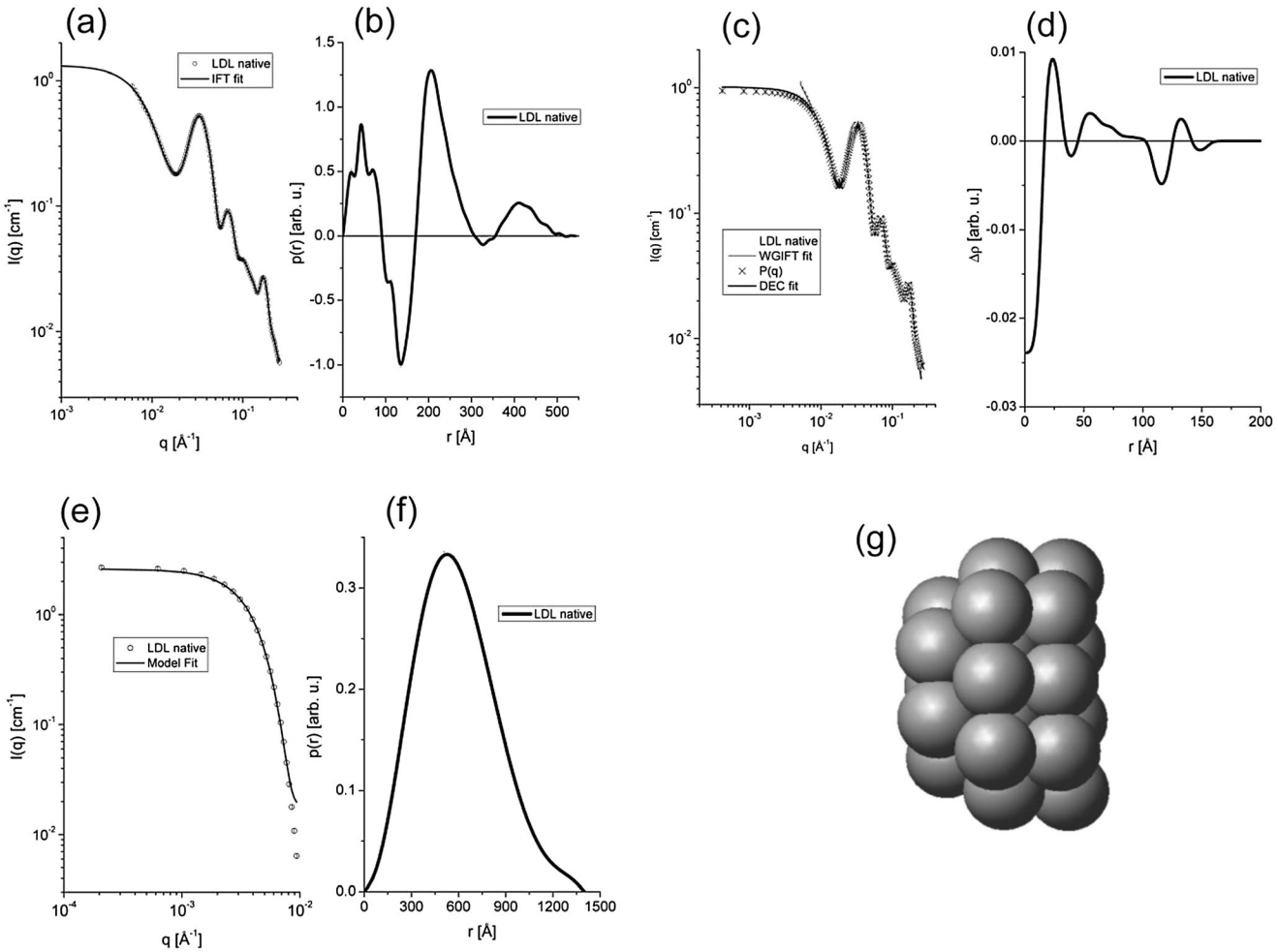

Fig. 2 Results for native LDL measured at 22 °C. IFT analysis: **a** experimental data (*circles*) and the IFT fit (*solid line*) and **b** pair distance distribution function $p(r)$. This *curve* indicates that the LDL nanoparticles have a diameter of ~310 Å ($p(r)$ curve approaching zero) and the maximum at round ~430 Å indicates the presence of a small fraction of aggregates. GIFT analysis: **c** GIFT fit (*dashed line*) and the calculated form factor (*crosses*). From this modeling, it is possible to obtain the structure factor and to estimate the size and shapes of the aggregates. The theoretical intensity for the aggregates is shown in **e** as *open circles* and the corresponding $p(r)$ curve in **f**. By using an ab initio modeling, it is possible to fit the data (*solid line* in **e**) and retrieve a 3D model for the aggregate, as shown in **g**. Note that the *spheres* in **g** have a diameter of 350 Å

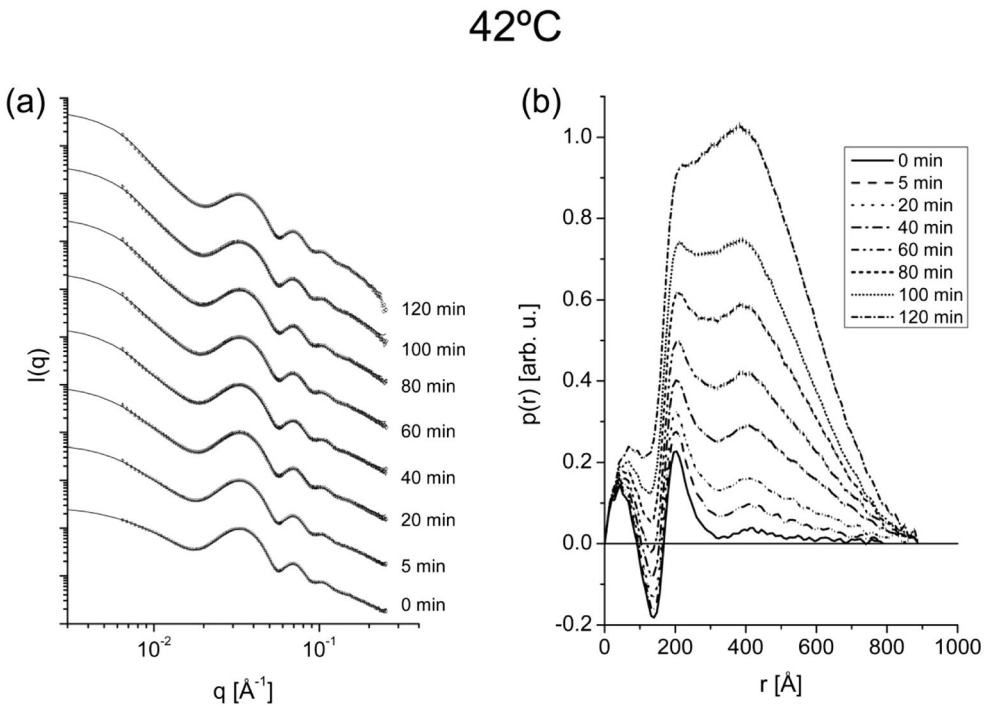

Fig. 3 IFT results for the LDL at 42 °C. **a** SAXS experimental data for different times (*open circles*) and theoretical fit (*solid lines*). **b** Pair distances distribution functions ($p(r)$). The increase of the height of the $p(r)$ curve for values larger than 300 Å indicates the increase of the contribution from the aggregates

In Eq. 10, the form factor $P_{MOD}(q)$ is the normalized-intensity form factor for the ellipsoid of revolution composed of multiple shells [1], with maximum radius R and polydispersity σ_R. Sc_1 and Sc_2 are scale factors, *Back* is a constant background, and $P_{Deb}(q)$ is the intensity form factor for the scattering from a flexible Gaussian chain with radius of gyration R_G^{Deb} [17]. All values of the parameters are optimized by using a partially constrained least squares procedure [18].

3 Results

The analysis of LDL samples started with the use of the IFT method. The obtained pair-distance distribution function for the native LDL is shown in Fig. 2a,b and the pair-distances distribution functions for the different temperature series are shown in Figs. 3–5. As can be seen from these analyses, the samples at 42 °C and 60 °C presented an evolution of the

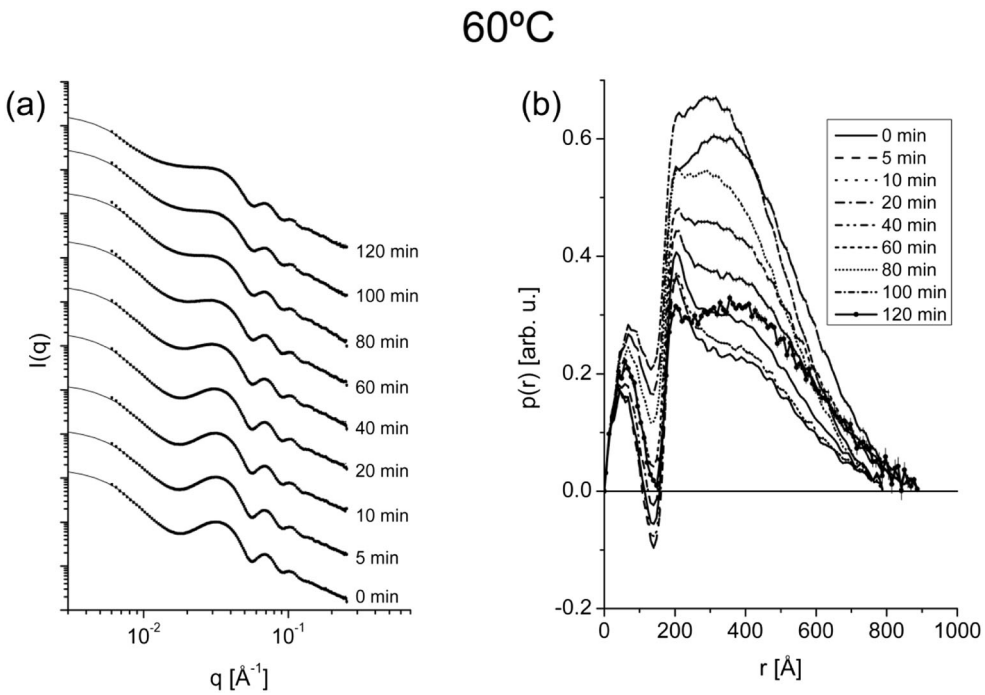

Fig. 4 IFT results for the LDL at 60 °C. **a** SAXS experimental data for different times (*open circles*) and theoretical fit (*solid lines*). **b** Pair distances distribution functions ($p(r)$). The increase of the height of the $p(r)$ curve for values larger than 300 Å indicates the increase of the contribution from the aggregates. For 120 min, one can see a decrease on the $p(r)$ height which can indicate either the breakage of the aggregates or precipitation of larger aggregates which effectively decreases the overall concentration of particle

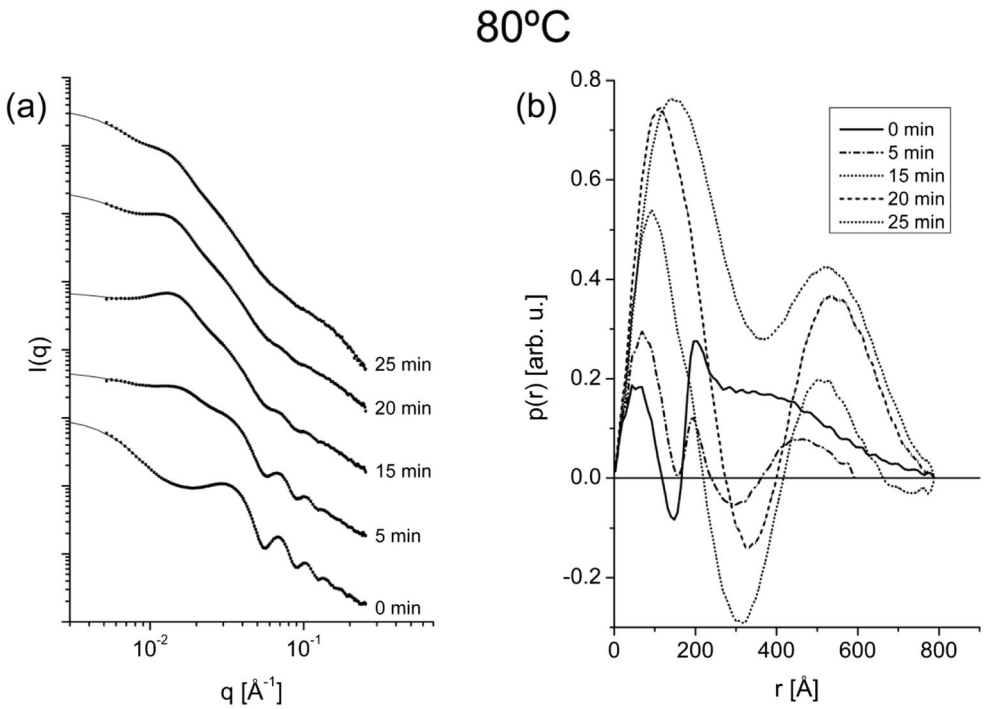

Fig. 5 IFT results for the LDL at 80 °C. **a** SAXS experimental data for different times (*open circles*) and theoretical fit (*solid lines*). **b** Pair distances distribution functions ($p(r)$). After the first $p(r)$ (at 0 min) which still resembles the overall shape of the LDL aggregates for the other samples (42 °C and 22 °C), the $p(r)$ curves completely change which can indicate the disruption of the LDL particles and the formation of different types of aggregates

fractions and types of aggregates over time. Interestingly, the lipoproteins seem to have an overall shape similar to that of the native (no modified) LDL. This can be inferred by the comparison of the initial part of the $p(r)$ functions in Figs. 3–5 and the Fig. 2b, which is the one of the native LDL at room temperature. These results and the systematic increase of the final region of the p(r) function for these temperatures indicate the formation of aggregates of LDL particles.

Table 1 Summary of results for the GIFT and Deconvolution methods for each dataset

Samples	Gift				Deconvolution			
	S_C^{agg}	R_G^{agg} [Å]	f_{LDL}^{num}	f_{agg}^{num}	Sc_2	R_G^{Deb}	R [Å]	σ_R [Å]
LDL 22 °C	1.5±0.6	329±5	0.997	0.003	0.19±0.1	54±1	155±1	14.4±0.3
LDL 42 °C 0 min	2.1±0.5	380±17	0.99	0.01	0.047±0.001	67±2	139±1	13.5±0.5
5 min	6.0±1.0	377±11	0.98	0.02	0.050±0.001	68±2	141±1	13.3±0.3
20 min	8.1±1.0	344±9	0.96	0.04	0.054±0.001	66±2	143±1	13.1±0.2
40 min	12.0±1.5	350±8	0.96	0.04	0.057±0.001	67±2	145±1	13.0±0.1
60 min	15.1±2.1	344±9	0.94	0.06	0.064±0.001	66±1	146±1	12.6±0.4
85 min	16.7±1.9	342±7	0.92	0.08	0.070±0.002	68±3	149±1	12.8±0.2
100 min	18.1±1.7	330±6	0.89	0.11	0.078±0.002	67±1	150±1	11.5±0.3
120 min	19.1±1.6	329±5	0.88	0.12	0.085±0.008	66±2	154±2	11.3±0.8
LDL 60 °C 0 min	9.0±0.5	327±4	0.94	0.06	0.15±0.02	147±2	161±3	15±2
5 min	8.2±0.5	329±5	0.94	0.06	0.13±0.01	117±8	162±2	16±2
10 min	8.1±0.6	339±5	0.94	0.06	0.16±0.02	132±8	167±2	14±2
20 min	9.1±0.7	328±5	0.93	0.07	0.21±0.03	136±7	167±3	16±2
40 min	8.0±0.8	346±6	0.93	0.07	0.44±0.03	178±7	170±4	15±2
60 min	8.1±0.7	337±6	0.91	0.09	0.71±0.05	190±9	170±15	16±3
80 min	7.1±0.5	349±5	0.89	0.11	1.16±0.08	240±11	171±11	14±5
100 min	6.8±0.5	352±5	0.91	0.09	0.96±0.05	224±7	172±20	15±6
120 min	6.0±0.3	377±4	0.96	0.04	0.45±0.02	167±4	167±3	16±2

The calculation of the numerical fractions for each sample is also presented (obtained with Eqs. 8 and 9, with α=2)

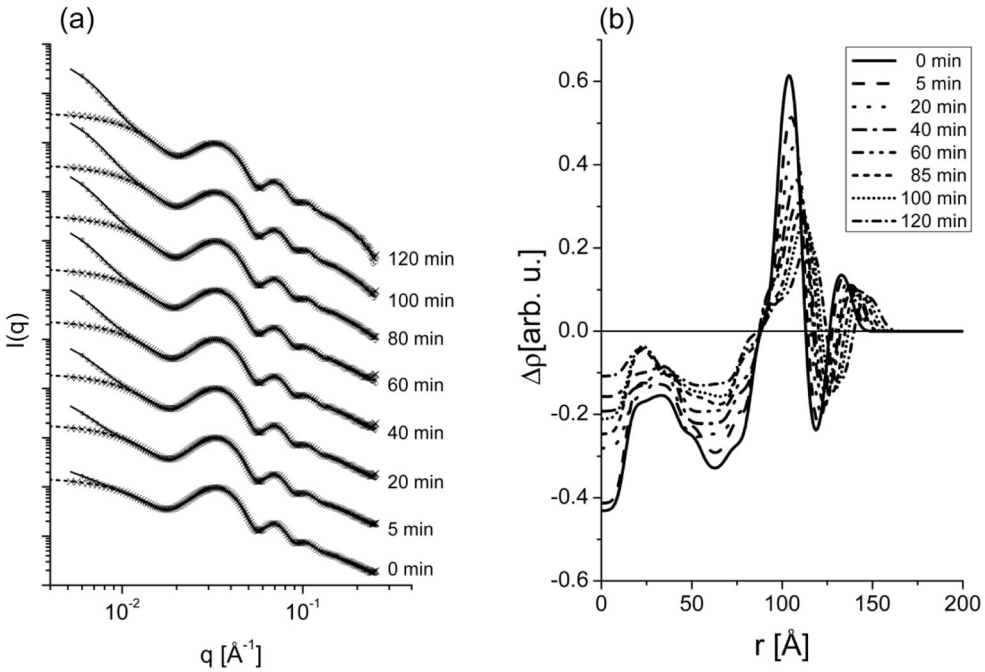

Fig. 6 GIFT and Deconvolution results for the LDL at 42 °C. **a** SAXS experimental data for different times (*open circles*), theoretical fits using Eq. 1 (*solid lines*), decoupled form factor (*crosses*), and the fit of the form factor by using the deconvolution procedure (*dash lines*). **b** Radial electron density profiles obtained for each temperature

For the sample at 80 °C, the first frame indicates that the LDL particles were assembled initially (maybe due to the heating of the sample inside the cell); but after 5 min, the SAXS profile and $p(r)$ curve changes drastically, probably indicating the disruption of the LDL particles and the formation of non-specific aggregates.

This initial analysis by using the IFT method suggested that, at the temperatures of 42 °C and 60 °C, the LDL lipoproteins (isolated and aggregated, but almost intact) are still present. However, the increase of the temperature may have changed its inner structure. In order to investigate this point, it was necessary to apply the GIFT method to decouple the particle's form factor and the system's structure factor. A summary of the results obtained with the GIFT method and deconvolution analysis is presented in Table 1. The fits by using the GIFT method are shown in Fig. 2 a, b, c for the native LDL at 22 °C, and in Figs. 6a and 7a for the data at 42 °C and 60 °C, respectively. As it can be seen, the fits by

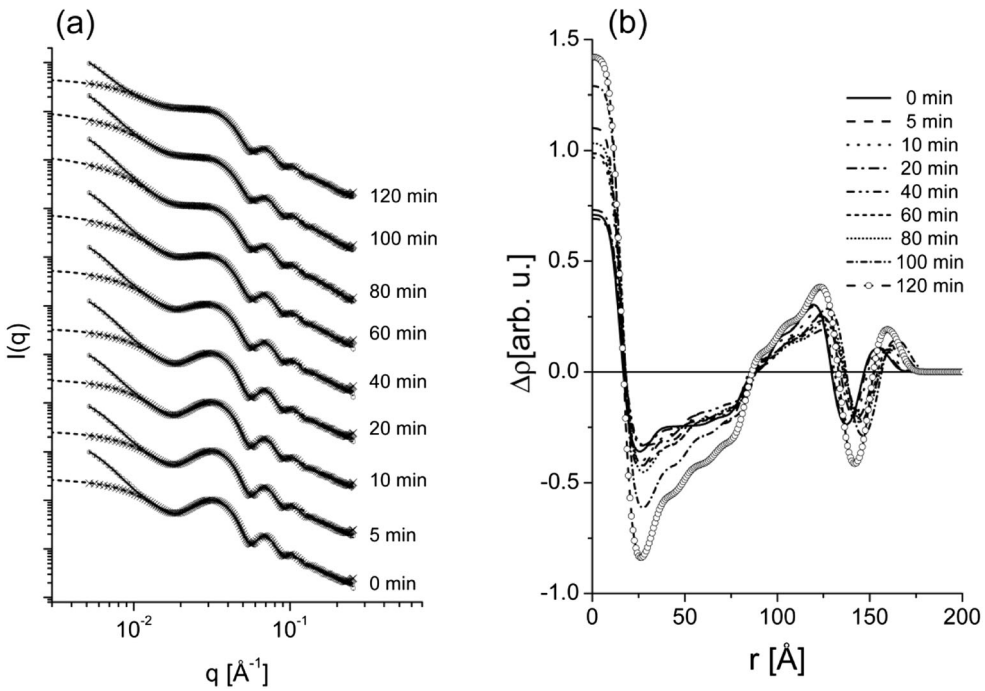

Fig. 7 GIFT and Deconvolution results for the LDL at 60 °C. **a** SAXS experimental data for different times (*open circles*), theoretical fits using Eq. 1 (*solid lines*), decoupled form factor (*crosses*), and the fit of the form factor by using the deconvolution procedure (*dash lines*). **b** Radial electron density profiles obtained for each temperature

using the proposed structure factor can describe the experimental data with high accuracy. Moreover, the corresponding form factor and structure factor for each dataset are obtained. From the structure factor, it was possible to obtain information about the aggregated state as well as the evolution of the corresponding fractions. In Fig. 2 a–f, the modeling of the form factor and structure factor, as well as the deconvolution procedure, is presented for the native LDL measured at 22 °C. In Figs. 8 a–f and 9 a–f, the aggregation results for the samples at 42 °C and 60 °C are shown. As it can be seen, it is possible to estimate the size of the aggregates (panels a, b) in each case and also obtain a representation of the shape of the aggregates (panel f). In addition, from the simple aggregation model described in section 2.4, one can calculate the evolution of the aggregates, i.e., their numerical fraction, volume fraction, and intensity fraction contributions (panels d–f). For the data at 42 °C (Fig. 8), one can see a monotonic increase of the forward scattering (panel c) indicating a continuous increase of the contribution of the aggregate. However, from Table 1, it is possible to see that the radius of gyration of the aggregate does not present a large variation; whereas, the scale factor S_C^{agg} shows a systematic increase. This can be converted in the aggregates numerical fractions, which are shown in panels d–f. It is interesting to note that even though the numerical fractions of the aggregates increases only up to 10 % (for 120 min at a constant temperature), the volume fractions of each population are similar at 60 min and the intensity fraction is dominated by the aggregates already from the first frame.

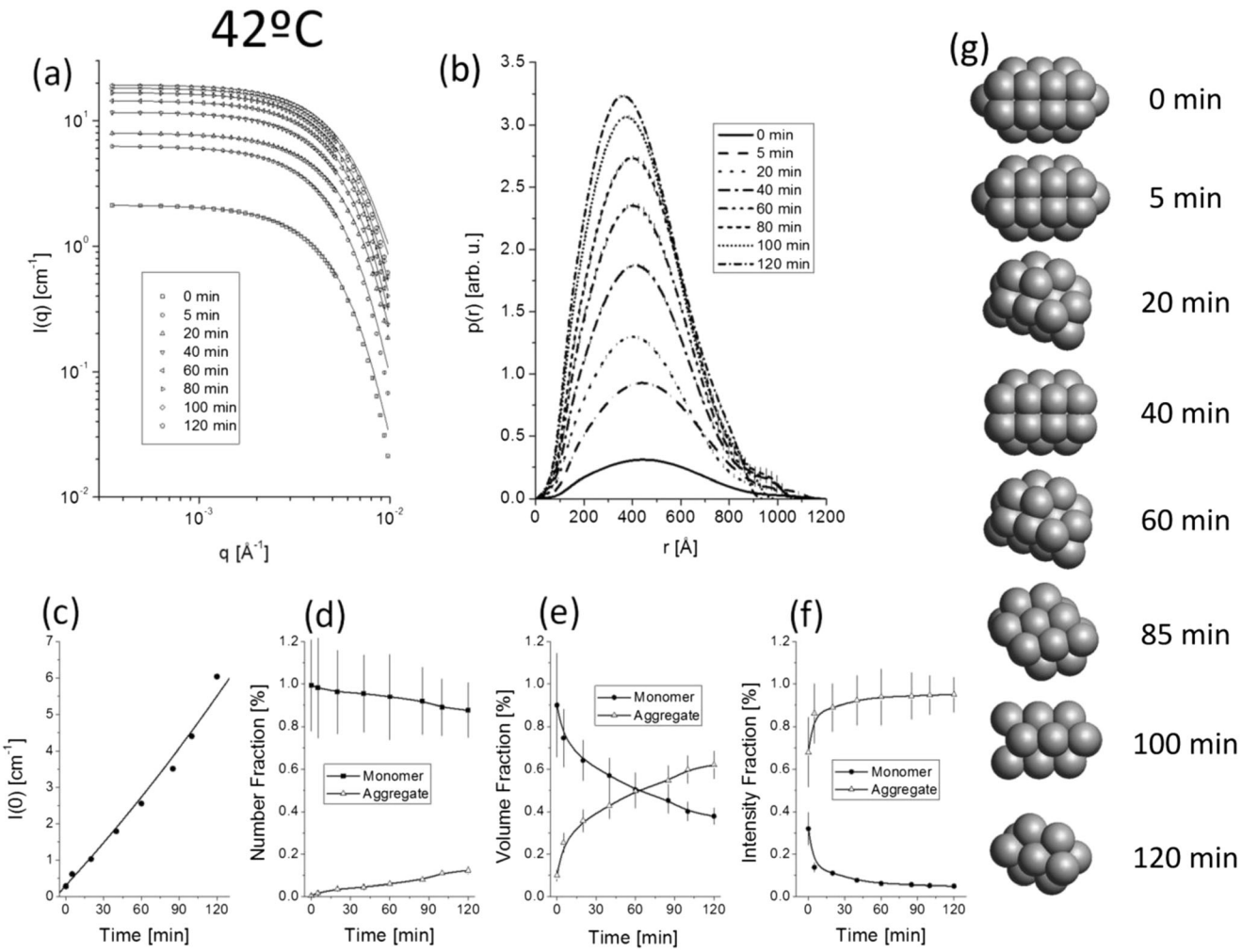

Fig. 8 Aggregation of LDL at 42 °C. IFT analysis: **a** Scattering intensity for the aggregates (*circles*) obtained from the GIFT method. The corresponding $p(r)$ function is shown in **b**. Calculation of the fractions: **c** forward scattering for the data collected at 42 °C (*circles*) indicating a monotonic increase of the intensity. This indicates a systematic increase of the contribution of the aggregates. In this graph, the line is for eye guiding. **d** Number fraction of monomers (*circles*) and aggregates (*open triangles*). **e** Volume fraction of monomers (*circles*) and aggregates (*open triangles*). **f** Intensity fraction of monomers (*circles*) and aggregates (*open triangles*). All fractions were calculated by using Eqs. 8 and 9 with the corresponding values for the exponent α. In these graph, the lines are for eye guiding. Modeling of the aggregates: by using ab initio modeling, it is possible to fit the data (*solid lines* in **a**) and retrieve a 3D model for the aggregates, as shown in **g** for each time. Note that the spheres in **g** have a diameter of 350 Å

Similar results were obtained for the data at 60 °C, as shown in Fig. 9. For this case, the numerical, volume, and intensity fractions of the isolated LDL and aggregates seem to be almost constant until 80 min. Differently from the data at 42°, the volume fraction of the isolated particles is always larger than the one of the aggregates. However, the intensity contribution is still dominated by that from the aggregates. The data after 100 min presents a strange behavior since the contribution from the aggregates seems to decrease. This can indicate the precipitation of the material due to formation of larger aggregates that are not visible by SAXS. This conclusion is also supported by the decrease of the $p(r)$ function height at larger values of r (Fig. 4b). All in all, the obtained results for the data at 60 °C presented more fluctuations than the one at 42 °C, which can be a consequence of the higher temperature of the system.

The fits from the deconvolution procedures and the corresponding electron-density profiles for each dataset are also presented. In Fig. 2 c,d, the results of the native LDL at 22 °C are shown. The modeling method provides a good fit to the experimental data (panel c) and the characteristic behavior for the electron-density profile [19]. It is interesting to analyze the differences induced by the temperature increase in the samples. When comparing the data at 22 °C and the ones at 42 °C and 60°, it is possible to see that the maximum at q~0.17 Å^{-1}, which is present at the room temperature SAXS data, disappears for the samples at higher temperature. This was already described in the literature as a phase transition of the lipidic content inside the lipoprotein, indicating a loss of the ordering [4–6, 19]. In a recent study, by using CryoEM, Molecular Dynamics, and SAXS [20, 21], it was shown that this maximum is

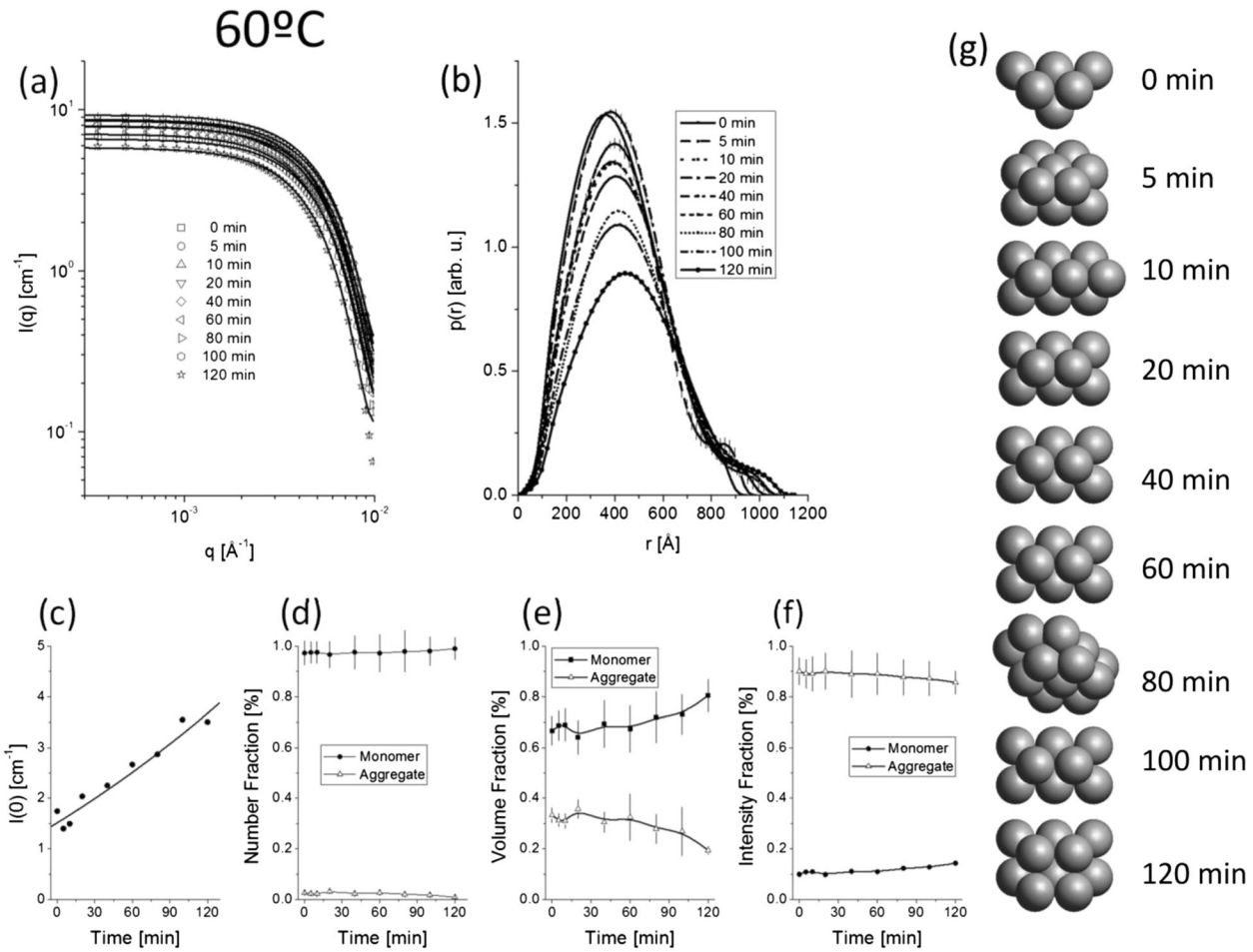

Fig. 9 Aggregation of LDL at 60 °C. IFT analysis: **a** scattering intensity for the aggregates (*circles*) obtained from the GIFT method. The corresponding $p(r)$ function is shown in **b**. Calculation of the fractions: **c** forward scattering for the data collected at 60 °C (*circles*) indicating a monotonic increase of the intensity. This indicates a systematic increase of the contribution of the aggregates. In this graph, the *line* is for eye guiding. **d** Number fraction of monomers (*circles*) and aggregates (*open triangles*). **e** Volume fraction of monomers (*circles*) and aggregates (*open triangles*). **f** Intensity fraction of monomers (*circles*) and aggregates (*open triangles*). All fractions were calculated by using Eqs. 8 and 9 with the corresponding values for the exponent α. In these graph, the lines are for eye guiding. Modeling of the aggregates: by using ab initio modeling, it is possible to fit the data (*solid lines* in **a**) and retrieve a 3D model for the aggregates, as shown in **g** for each time. Note that the *spheres* in **g** have a diameter of 350 Å

related to the ordering of the cholesterol molecules in the inner core of the LDL particle. This loss of ordering and "melting" of the inner core is clearly indicated by the electron density profiles, as shown in our experiment (see Figs. 6 and 7). By comparing the electron-density profile ($\Delta\rho$) obtained with the native LDL at room temperature (Fig. 2d) with those obtained at 42 °C and 60 °C (Figs. 6b and 7b), it is possible to see that the maxima in $\Delta\rho$ are broader in the experiments at higher temperatures. In the case of the native LDL, we observed a periodic behavior of the radial electron-density profile at small values of r. This indicates the existence of a local ordering and gives rise to the maximum in the scattering profile $I(q)$ at q~0.17 Å^{-1}. In the data acquired at 42 °C and 60 °C, this well-defined periodic behavior is lost, indicating the loss of ordering inside the particle. The electron-density profiles obtained for each temperature show remarkable differences, which may indicate important differences in the inner arrangement of the lipoproteins.

The contribution from flexible parts in the scatter system is also an interesting point. The radius of gyration of the Debye chain (R_G^{Deb}) obtained with the sample at 42 °C is slightly larger than the one obtained at 22 °C (Table 1). This indicates a small increase of the particle's shape fluctuation, and eventually, a signature of flexible parts on the particle. However, there is a systematic increase on the scale factor S_{C_2} , which indicates that these contributions become more and more important as time goes by. For the data at 60 °C, on the other hand, the parameters that characterize the flexible contribution to the scattering change drastically. Our results show an important and systematic increase on the R_G^{Deb} and also on S_{C_2} which indicates that the size of the flexible regions on the lipoprotein (probably the protein apoB on its surface) and its contribution to the total intensity increases as time goes by. A possible explanation for this result can be attributed to the detachment of some regions of the the apoB-100 from the particle, causing an important increase of the R_G^{Deb}. This effect is probably due to the effect of the high temperature.

4 Summary and Conclusions

In this work, it is presented a controlled and systematic study of LDL internal structure and particle's aggregation due to changes in the sample's temperature. A complete analysis and modeling procedure is proposed, permitting the retrieval of structural parameters for the LDL particles, shape and evolution of the aggregates, and also the fractions of the isolated and aggregated states. By the use of a decoupling procedure and the simple aggregation model, the evolution of the fraction of the two species (isolated particles and aggregates) could be retrieved as a function of temperature. The aggregates overall shapes could be obtained by the use of ab initio modeling of the scattering data. For the isolated particles, the use of the deconvolution modeling on the scattering data allowed the calculation of the corresponding radial electron-density profile, which is directly related to the particle's internal structure. The loss of internal ordering, which is associated to a phase transition on the cholesterol, occurred when varying the temperature from 22° to 42° (and above) and could be explained by the important change in the electron-density profiles. Also, by this analysis, it was possible to follow the changes in the LDL internal structure due to the increase of temperature. Finally, the use of the Debye chain in the model provided a direct indication of the degree of the flexibility and conformation of the apoB-100. The results demonstrated a remarkable and systematic increase on the degree of flexibility of the protein, probably due to structural changes induced by temperature.

The procedure presented in this work provides a general framework that can be used on the study of dynamical processes in lipoprotein systems, allowing the online and in situ monitoring and modeling of the system. Also, since the calculated electron-density profiles are a direct indication of the average distribution of the components inside the lipoproteins, they can be used to check and validate MD simulations for systems of lipoproteins. The size and shape of the aggregates, as well as the evolution of the fractions of each species, can be used as guide for aggregation models of lipoproteins.

Acknowledgments This study was supported by The National Council for Scientific and Technological Development (CNPq), São Paulo Research Foundation (FAPESP), and National Institute of Science and Technology of Complex Fluids (INCT-FCx). The authors acknowledge the Brazilian Synchrotron Light Laboratory for the SAXS data acquisition (proj. # SAXS1-10713). The authors thank Dr. Priscila R. Santos for the support on sample preparation and data acquisition.

Author Contributions The manuscript was written through contributions of all authors. All authors have given approval to the final version of the manuscript.

Appendix 1

a) Derivation of Eqs. 8 and 9

The scattering intensity for a system composed of two populations is given by:

$$I(0)_{tot} = c_{LDL}(\Delta\rho)^2 V_{LDL}^2 + c_{agg}(\Delta\rho)^2 V_{agg}^2 \quad \text{(a1)}$$

$$I(0)_{tot} = c_{LDL}(\Delta\rho)^2 V_{LDL}^2 \left(1 + S_C^{agg}\right) \quad \text{(a2)}$$

where,

$$S_C^{agg} = \frac{c_{agg} V_{agg}^2}{c_{LDL} V_{LDL}^2} \quad \text{(a3)}$$

The fraction of the particles in each population is the ratio between the number of particles in one population divided by the total number of particles weighted in a given way. For the number fraction, it is not necessary to use weighting, for the volume fraction one has to weight by the volume and for the intensity fraction the weighting function is the volume square. It is possible to write a single formula for the fractions if one uses as weighting function the volume to the power 2-α :

$$f^i_{LDL} = \frac{c_{LDL}(\Delta\rho)^2 V_{LDL}^{2-\alpha}}{c_{LDL}(\Delta\rho)^2 V_{LDL}^{2-\alpha} + c_{agg}(\Delta\rho)^2 V_{LDL}^{2-\alpha}}$$

$$f^i_{LDL} = \frac{c_{LDL}V_{LDL}^{2-\alpha}}{c_{LDL}V_{LDL}^{2-\alpha} + c_{agg}V_{LDL}^{2-\alpha}} = \frac{c_{LDL}V_{LDL}^{2-\alpha}/c_{LDL}V_{LDL}^{2-\alpha}}{\left(c_{LDL}V_{LDL}^{2-\alpha} + c_{agg}V_{LDL}^{2-\alpha}\right)/c_{LDL}V_{LDL}^{2-\alpha}} = \frac{1}{1+\frac{c_{agg}V_{agg}^{2-\alpha}}{c_{LDL}V_{LDL}^{2-\alpha}}} \tag{a4}$$

$$f^i_{LDL} = \frac{1}{1+S_C^{agg}\frac{V_{LDL}^2}{V_{agg}^2}\frac{V_{agg}^{2-\alpha}}{V_{LDL}^{2-\alpha}}} = \frac{1}{1+S_C^{agg}\left(\frac{V_{agg}}{V_{LDL}}\right)^{-\alpha}} \Rightarrow f^i_{LDL} = \frac{1}{1+S_C^{agg}\left(\frac{V_{LDL}}{V_{agg}}\right)^{\alpha}}$$

For the fraction of aggregates weighted by the volume to the power 2-α, simple algebraic operations lead to,

$$f^i_{agg} = \frac{1}{1+\frac{1}{S_C^{agg}}\left(\frac{V_{agg}}{V_{LDL}}\right)^{\alpha}} \tag{a5}$$

By inspection, one can show that $f^i_{LDL}+f^i_{agg}=1$.

If one assumes that the LDL particles and aggregates have a globular shape, the volume scales with the cube of the particle radius of gyration, so

$$f^i_{LDL} = \frac{1}{1+S_C^{agg}\left(\frac{\left(R_G^{LDL}\right)^3}{\left(R_G^{agg}\right)^3}\right)^{\alpha}} = \frac{1}{1+S_C^{agg}\left(\frac{R_G^{LDL}}{R_G^{agg}}\right)^{3\alpha}} \tag{a6}$$

$$f^i_{agg} = \frac{1}{1+\frac{1}{S_C^{agg}}\left(\frac{R_G^{agg}}{R_G^{LDL}}\right)^{3\alpha}} \tag{a7}$$

For the numerical fraction, i="num" and $\alpha=2$; for volume fraction, i="vol" and $\alpha=1$; and for the intensity fraction, i="int" and $\alpha=0$.

References

1. C.L.P. Oliveira, P. Santos, A. Monteiro, A.M. Figueiredo Neto, Effect of oxidation on the structure of human low and high density human lipoproteins. Biophys. J. **106**, 2595–2605 (2014)
2. R. Prassl, M. Pregetter, H. Amenitsch, M. Kriechbaum, R. Schwarzenbacher, J.M. Chapman, P. Laggner, Low density lipoproteins as circulating fast temperature sensors. Plos One **3**, e4079 (2008)
3. N.F. Galeano, M. Al-Haideri, F. Keyserman, S.C. Rumsey, R.J. Deckelbaum, Small dense low density lipoprotein has increased affinity for LDL receptor-independent cell surface binding sites: a potential mechanism for increased atherogenicity. J. Lipid Res. **39**, 1263–1273 (1998)
4. P. Laggner, G. Degovics, K.W. Muller, O. Glatter, O. Kratky, G. Kostner, A. Holasek, Molecular packing and fluidity of lipids in human-serum low-density lipoproteins. Hoppe-Seylers Z Physiol Chem **358**, 771–778 (1977)
5. D. Atkinson, R.J. Deckelbaum, D.M. Small, G.G. Shipley, Structure of human-plasma low-density lipoproteins—molecular-organization of central core. Proc. Natl. Acad. Sci. USA **74**, 1042–1046 (1977)
6. R.J. Deckelbaum, G.G. Shipley, D.M. Small, Structure and interactions of lipids in human-plasma low-density lipoproteins. J. Biol. Chem. **252**, 744–754 (1977)
7. S. Jayaraman, D. Gantz, O. Gursky, Structural basis for thermal stability of human low-density lipoprotein†. Biochemistry **44**, 3965–3971 (2005)
8. M. Lu, D.L. Gantz, H. Herscovitz, O. Gursky, Kinetic analysis of thermal stability of human low density lipoproteins: a model for LDL fusion in atherogenesis. J. Lipid Res. **53**, 2175–2185 (2012)
9. R.J. Havel, H.A. Eder, J.H. Bragdon, Distribution and chemical composition of ultracentrifugally separated lipoproteins in human serum. J. Clin. Invest. **34**, 1345–1353 (1955)
10. G. Kellermann, F. Vicentin, E. Tamura, M. Rocha, H. Tolentino, A. Barbosa, A. Craievich, I. Torriani, The small-angle X-ray scattering beamline of the brazilian Synchrotron Light Laboratory. J. Appl. Crystallogr. **30**, 880–883 (1997)
11. L.P. Cavalcanti, I.L. Torriani, T.S. Plivelic, C.L.P. Oliveira, G. Kellermann, R. Neuenschwander, Two new sealed sample cells for small angle X-ray scattering from macromolecules in solution and complex fluids using synchrotron radiation. Rev. Sci. Instrum. **75**, 4541–4546 (2004)
12. A.P. Hammersley, S.O. Svensson, M. Hanfland, A.N. Fitch, D. Hausermann, Two-dimensional detector software: from real detector to idealised image or two-theta scan. High Pressure Res. **14**, 235–248 (1996)
13. O. Glatter, A new method for the evaluation of small-angle scattering data. J. Appl. Crystallogr. **10**, 415–421 (1977)
14. C.L.P. Oliveira, M.A. Behrens, J.S. Pedersen et al., A SAXS study of glucagon fibrillation. J. Mol. Biol. **387**, 147–161 (2009)
15. J.S. Pedersen, S. Hansen, R. Bauer, The aggregation behavior of zinc-free insulin studied by small-angle neutron-scattering. Eur. Biophys J. Biophys. Lett. **22**, 379–389 (1994)

16. D.I. Svergun, Restoring low resolution structure of biological macromolecules from solution scattering using simulated annealing. Biophys. J. **76**, 2879–2886 (1999)
17. P. Debye, Molecular-weight determination by light scattering. J. Phys. Colloid Chem. **51**, 18–32 (1947)
18. C.L.P. Oliveira, B.B. Gerbelli, E.R.T. Silva, F. Nallet, L. Navailles, E.A. Oliveira, J.S. Pedersen, Gaussian deconvolution: a useful method for a form-free modeling of scattering data from mono- and multilayered planar systems. J. Appl. Crystallogr. **45**, 1278–1286 (2012)
19. P. Laggner, K.W. Muller, Structure of serum-lipoproteins as analyzed by X-ray small-angle scattering. Q. Rev. Biophys. **11** (1978)
20. G. Ren, G. Rudenko, S.J. Ludtke, J. Deisenhofer, W. Chiu, H.J. Pownall, Model of human low-density lipoprotein and bound receptor based on CryoEM. Proc. Natl. Acad. Sci. USA **107**, 1059–1064 (2010)
21. Y. Liu, D. Luo, D. Atkinson, Human LDL core cholesterol ester packing: three-dimensional image reconstruction and SAXS simulation studies. J. Lipid Res. **52**, 256–262 (2011)